ELSEVIER

Neurobiology of Aging, Vol. 19, No. 5, pp. 479–485, 1998

0197-4580/98 $19.00 + .00

PII:S0197-4580(98)00081-5

Magnetic Resonance Imaging of Anatomic and Vascular Characteristics in a Canine Model of Human Aging

MIN–YING SU,*[1] ELIZABETH HEAD,† WILLIAM M. BROOKS,‡ ZHIHENG WANG,* BRUCE A. MUGGENBURG,¶ GINA E. ADAM,§ ROBERT SUTHERLAND,§ CARL W. COTMAN,† AND ORHAN NALCIOGLU*

**Health Sciences Research Imaging Center and †Institute for Brain Aging & Dementia, University of California, Irvine, CA 92697; ‡Center for Non-Invasive Diagnosis and Department of Neurosciences, and §Department of Psychology, University of New Mexico, Albuquerque, NM 87131; and ¶Lovelace Respiratory Research Institute, Albuquerque, NM 87185*

Received 24 March, 1998; Revised 26 June 1998; Accepted 19 July 1998

SU, M-Y., E. HEAD, W. M. BROOKS, Z. WANG, B. A. MUGGENBURG, G. E. ADAM, R. J. SUTHERLAND, C. W. COTMAN, AND O. NALCIOGLU. *MRI of anatomic and vascular characteristics in a canine model of human aging.* NEUROBIOL AGING **19**(5) 479–485, 1998.—Dogs exhibit both neuroanatomical and cognitive changes as a function of age that parallel those seen in aging humans. This study describes in vivo changes in neuroanatomical and cerebrovascular characteristics of the canine brain as a function of age in a group of dogs ranging from 4 to 15 years old. Dynamic contrast-enhanced magnetic resonance imaging (MRI) was used to measure the kinetics of contrast agents in the brain. Measures of vascular volume and blood-brain barrier (BBB) permeability were derived from a pharmacokinetic analysis. Cortical atrophy and ventricular enlargement were characteristic features of the aged canine brain. Vascular volume did not vary as a function of age and BBB permeability exhibited a nonsignificant increasing trend with age. However, BBB dysfunction was detected in one middle-aged dog that in addition to having unusually large ventricles, demonstrated an early onset of diffuse senile plaques at postmortem. These findings indicate that BBB dysfunction detected by magnetic resonance imaging may be useful for predicting and potentially diagnosing early pathological conditions. © 1998 Elsevier Science Inc.

Aging Dog Anatomic MRI Dynamic contrast-enhanced MRI Atrophy Vascular volume BBB leakage Pharmacokinetic analysis β-amyloid Senile plaques

NORMAL aging and development of Alzheimer's disease (AD) are associated with anatomical and functional changes in the brain [see review (7,12)]. Normal aging is associated with brain atrophy and ventricular enlargement, perivascular space enlargement and white-matter lesions. Functionally, aging is associated with cerebral blood-flow reduction and decreased glucose and O_2 metabolism. However, the reduction of cerebral blood flow could be attributed, at least in part, to associated brain atrophy (25). Therefore, specific functional information obtained from a well-defined anatomical region would be more valuable than global measures. In practice, however, this problem is difficult to solve because it is greatly limited by the lack of co-registration of the brain position between two modalities for structural (magnetic resonance imaging (MRI)) and functional single photon emission computed tomography (SPECT) or positron emission tomography (PET)) imaging. In recent years, a new technique, dynamic contrast-enhanced MRI, has been widely applied for tumor imaging to study vascular characteristics under the same conditions as anatomical MRI scans. In addition, the kinetics of MR contrast agents can be analyzed with a pharmacokinetic model to derive vascular volume and permeability measures (24,27). Therefore, we used this MRI technique to measure both anatomical and vascular characteristics in the same imaging study to reveal regional information.

MRI techniques, in theory, can be used to bridge the gap between postmortem anatomical studies and in vivo measures of brain function. One form of pathology commonly seen in brain tissue and cerebral vessels in both normal and pathological aging brain is the deposition of β-amyloid in the form of senile plaques. Amyloid angiopathy is associated with β-amyloid that interacts with endothelial cells and can potentially cause damage to the blood-brain barrier (BBB) (23). Damaged endothelium may exhibit enhanced vasoconstriction leading to chronic cerebral hypoperfusion. Furthermore, recent studies show evidence of damaged smooth muscle cells of the cerebral vessels producing β-amyloid (8,10,19,26,29). Similar neuropathology findings are observed in the canine (9,28); deposition of β-amyloid is a common feature in the brain of the aged dog. We propose that β-amyloid associated vascular dysfunction may also exist in the canine and it may be possible to detect this form of pathology using MRI techniques.

[1] Address correspondence to: Min-Ying Su, Ph.D., Research Imaging Center, Irvine Hall 164, University of California, Irvine, CA 92697-5020; E-mail: msu@uci.edu

In the current study, we applied MRI techniques to investigate age related neuroanatomical and cerebrovascular changes in the canine, which is suggested to be an animal model of human aging and dementia (4,5,6). The advantage to using the dog model is that the time delay between the MRI scans and neuropathology studies can be controlled and minimized, enhancing our understanding of the relationships between these measures. A group of canines with ages ranging from 4 to 15 years were given MR scans to measure neuroanatomical and cerebrovascular characteristics, including cerebral vascular volume and BBB permeability. Preliminary data describing the relationship between amyloid pathology and both anatomic and vascular characteristics will also be discussed.

MATERIALS AND METHODS

Subjects

MRI examination was performed on 18 beagle dogs from the animal facility at the Lovelace Respiratory Research Institute in Albuquerque, NM. The dogs consisted of 9 males and 9 females ranging in age from 4–15 years and weighing between 4 and 15 kg. All dogs had undergone cognitive testing during a 2-year period prior to the imaging study (14).

Cognitive Testing

The test apparatus and cognitive tasks have been described in more detail elsewhere (14,22). All cognitive testing took place in a modified Wisconsin General Test Apparatus that consisted of a large wooden box with stainless steel bars serving as the front. The bars could be raised or lowered to allow dogs to reach a moveable presentation tray. The tray was made of black plexiglas with three recessed food wells: two lateral wells and one medial well. A barrier with a one-way mirror separated the experimenter from the dog.

Dogs were given six behavioral tasks: reward- and object-approach learning, object-discrimination learning and reversal, long-term retention of a reversal problem, and size-discrimination learning. The first four tests occurred 2 years prior to the MR scan and the last two tasks were given within 2 months of the MR scans. For all tasks, dogs were given ten trials per day with a 1.5-min intertrial interval. Dogs were given a new task after reaching one of two criteria: 9/10 correct on one day or 8/10 correct for 2 days in a row. The food reward consisted of one teaspoon (approximately 4 mL) of wet dog food formed into a ball.

Reward- and object-approach learning tasks are part of our standard protocol for teaching dogs how to work in the test apparatus. Reward-approach learning involves showing the dogs the presentation tray with a food reward in either the left or right well. Dogs are required to visually locate and obtain the food reward. Object-approach learning requires that dogs displace an object to obtain the food reward. Object-discrimination learning involves presenting dogs with two different objects simultaneously, with one object being rewarded consistently on all trials. The correct response is to select the rewarded object. Object-reversal learning is identical to discrimination learning but the reward contingencies have been reversed; the previously correct object is now the incorrect object. Dogs must inhibit their response to the previously correct object and learn to respond to the previously incorrect object. After a 2-year interval, the dogs were retested on the reversal problem to measure long-term retention. Following retention testing, dogs were given a size-discrimination learning task that was identical to object-discrimination learning but the two objects differed only in size.

MRI

The MRI study took place at the Center for Non-Invasive Diagnosis, University of New Mexico, Albuquerque, NM. MRI experiments were performed using a clinical GE Signa 1.5 T scanner with a linear head coil. Each dog was first sedated with acepromazine (2 cc), then anesthetized by inhalation of Isoflurane. After the animal was intubated, anesthesia was maintained at 1.5–2% through the experimental period. An i.v. catheter was placed in the lateral saphenous vein of the hind leg to allow the maintenance of a slow drip of lactated Ringers solution throughout the scanning procedures. In addition, the i.v. line was used to inject contrast agent during the study. Monitoring devices were put in place to measure the heart rate, blood pressure, and blood oxygenation levels during the anesthesia.

A set of three-dimensional (3D) images across the whole brain were acquired using a spoiled gradient recall (SPGR) pulse sequence to obtain detailed anatomic images. The parameters were: repetition time (TR) = 40 ms, echo time (TE) = 9 ms, flip angle = 40°, slice thickness = 1 mm, 124 slices, field of view (FOV) = 12 × 9 cm, matrix size = 256 × 192, 3/4 phase encoding, number of excitations (NEX) = 3, and the total scan time was approximately 37 min. Four slices, each 6 mm thick, were obtained from the frontal cortex, thalamus, hippocampus, and cerebellum for the dynamic contrast enhancement study. A spin-echo pulse sequence (with TR/TE = 117/14 ms, FOV = 12 × 9 cm, matrix size = 256 × 128, NEX = 1) was applied to simultaneously acquire T_1-weighted images from these four brain regions. The dynamic acquisition mode was achieved using the scanner graphical prescription function. In a single acquisition, one image was obtained at each of four slice locations, then the next acquisition was used to obtain the next set of four images and so on. The temporal resolution was 15 s using this protocol for dynamic imaging.

After four baseline images had been acquired from each brain region, the contrast agent Gd-DTPA, (Magnevist®, 0.15 mmol/kg) was injected. The injection of Gd-DTPA with 3 cc saline for flush was timed to be given in exactly 30 sec in every animal, to keep the arrival of contrast agent into the brain consistent. After the first sequence was finished, the sequence was repeated two more times to measure the enhancement kinetics up to 12 min. All studies were approved by the Lovelace Respiratory Research Institute Animal Research Committee and University of New Mexico Health Sciences Center Laboratory Animal Care and Use Committee. At the conclusion of the imaging studies, dogs were allowed to recover from the anesthesia. Over the next 2–14 days, they were sacrificed with an overdose of Nembutal and brains were collected for postmortem neuroanatomical analysis (14).

Immunohistochemistry

Brain tissues were fixed in 4% paraformaldehyde at 4°C for 72 to 80 h. The tissue was transferred into phosphate-buffered saline (PBS), pH 7.4, with 0.02% sodium azide and stored at 4°C. Amyloid was detected using a rabbit polyclonal antibody, designated β42, raised against a synthetic β-amyloid peptide containing amino acids 1 through 42 (4).

Fifty-μm vibratome sections were taken from the dorsolateral prefrontal cortex, the entorhinal cortex, the occipital cortex and the parietal cortex according to the canine brain atlas described by Kreiner (20). Sections were pretreated for 4 min with 90% formic acid prior to overnight incubation at room temperature in 42 (1:500) in Tris-saline with 2.0% bovine serum albumin (BSA) and 0.1% Triton X-100. For each region examined, all 20 subjects were stained simultaneously in one immunocytochemistry run to maintain consistent reagent and dilution parameters and to reduce

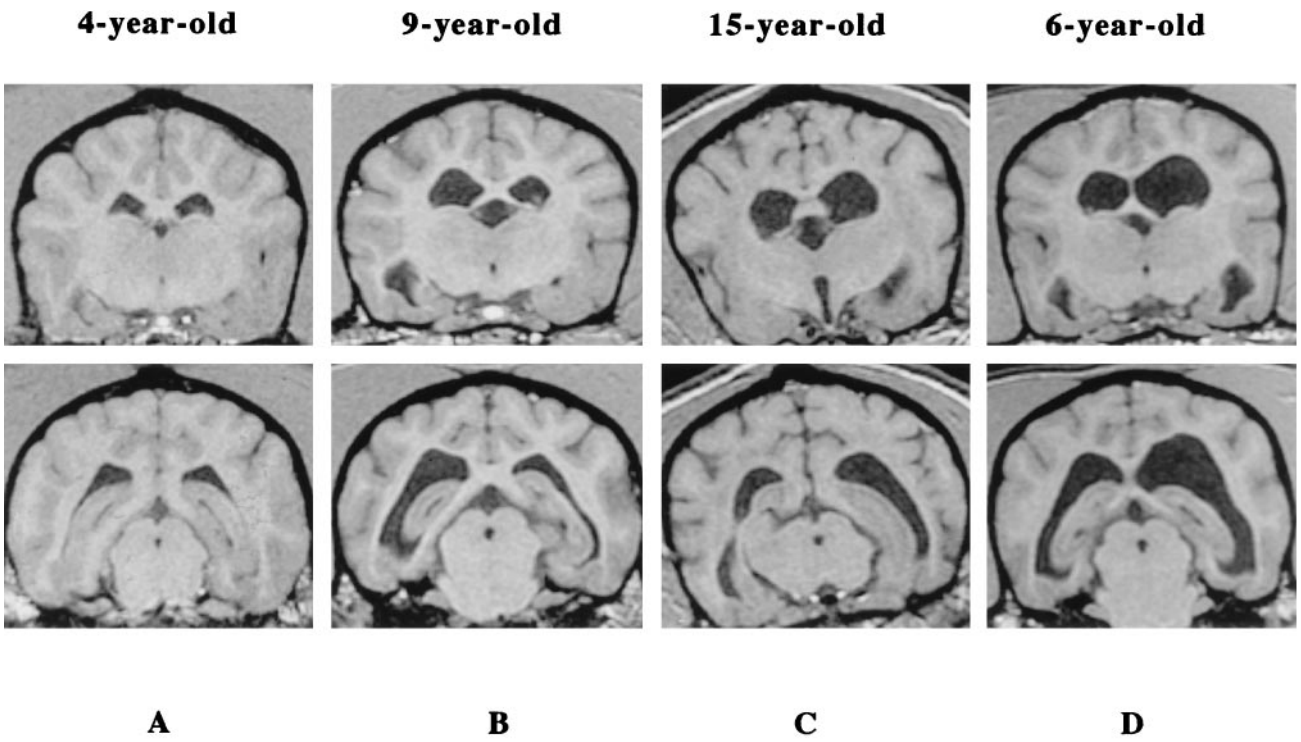

FIG. 1. MR images from a (*A*) 4-year-old, (*B*) 9-year-old, (*C*) and 15-year-old dog taken from locations through thalamus and hippocampus. The old dogs show marked increases in ventricular volume and cortical atrophy (with deep gyri and widened sulci). One middle-aged dog (6-year-old, *D*) who showed unusually large ventricles also had BBB dysfunction and early onset β-amyloid accumulation.

variability. Staining runs with all 20 subjects were repeated to obtain two samples from each brain region. Bound antibody was detected using a biotinylated anti-rabbit ABC peroxidase kit from Vector Labs (Burlingame, CA). β42 was visualized using a DAB substrate kit from Vector Labs (Burlingame, CA).

Data Analysis

For behavioral test analysis, error scores were used as dependent variables. Error scores were calculated by adding the number of errors each dog committed each day across all the days of testing up to and including the day criterion was met. A detailed analysis of age effects on the six behavioral tasks and relationship to β-amyloid pathology is reported elsewhere (14). For MR analysis, a Sun Sparc 20 workstation with programs written in Matlab was used for data analysis. To obtain anatomical measures, the total cerebral volume, the cerebral tissue volume (gray matter and white matter), the volume of the lateral ventricles, and the cerebellar volume were measured from the 3D anatomic images in each dog. Some images taken with the 3D SPGR pulse sequence are shown in Fig. 1. The volume of the region-of-interest (ROI) was measured by operator-defined and computer-assisted analysis. An analysis program was developed to outline the boundary of a region by manually clicking the mouse button on the image. Then within the outlined region we can set threshold values to arbitrarily select pixels with the signal intensity within a certain gray level range.

The cerebral area in each image was manually outlined, then the total cerebral volume was calculated by summing over the outlined regions from all images taken across the entire cerebral region. The region included all brain tissue (gray matter and white matter) as well as sulci, gyri, and atrophy (filled with cerebrospinal fluid (CSF)). In the images the white matter appeared with high gray level signal intensity, CSF had the lowest signal intensity, and the gray matter appeared with moderate signal intensity. Figure 2 shows the signal intensity histogram of pixels within the cerebral region outlined from one image. The CSF has the lowest intensity, and the two peaks represent the gray matter and the white matter. A threshold gray level of 99 was set to differentiate the CSF from the brain tissue (gray matter and white matter). After excluding the CSF from the total cerebral volume, the volume of the brain tissue was calculated. To measure the lateral ventricle volume, two ROIs covering the left and right lateral ventricles in each image were manually outlined and the area calculated. The lateral ventricle volume was calculated by summing over the volumes of all outlined regions. The total cerebellar volume was measured by summing the manually outlined cerebellum regions from the 3D images.

In each dog, the kinetics of Gd-DTPA were measured from brain tissue, i.e., only from the gray matter and white matter but not the CSF. Based on the corresponding anatomic images a segmentation algorithm was applied to define and exclude the pixels filled with CSF in the analysis of dynamic images. Then in each of the dynamic images acquired before and after injection of Gd-DTPA, a mean signal intensity was calculated from the remaining pixels. The precontrast signal intensity was subtracted from the postcontrast signal intensity at every time point to obtain the signal enhancement kinetics. The signal enhancement reflected the amount of contrast agent in the region, which in turn was dependent on the blood volume and the leakage of the agent into the interstitial brain tissue from the damaged BBB. The distribution of contrast agents in these two compartments was separated using a pharmacokinetic modeling analysis (24). For this analysis we used the kinetics taken from a 4-year-old dog as a standard

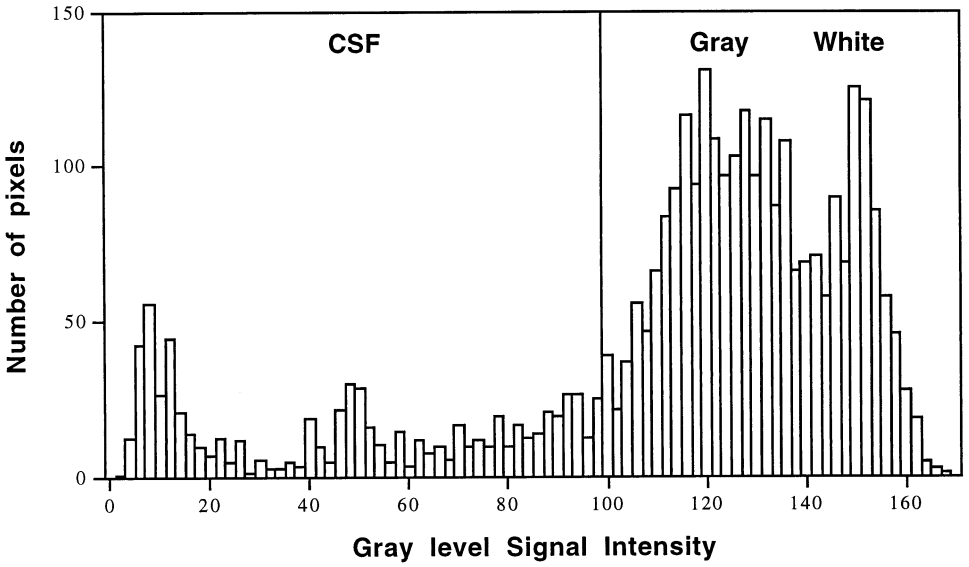

FIG. 2. The signal-intensity histogram of pixels within the cerebral region of an anatomic image acquired using the 3D SPGR pulse sequence. The CSF has the lowest signal intensity. The two peaks represent the gray matter and white matter, which are overlapped thus can not be clearly separated. However, separation between CSF and gray matter can be easily achieved by defining a threshold value of 99.

reference for vascular kinetics and based on this, the kinetics measured in the other dogs were separated into vascular and interstitial components. Enhancement in the vascular kinetics reflected contrast agent concentration in the vascular space, which in turn was proportional to vascular volume and was defined as the vascular volume index. The enhancement in the interstitial kinetics was related to the total amount of contrast agent passing through the BBB into the interstitial space. The ratio between the interstitial enhancement to the vascular enhancement was a measure of the fraction of agents that diffused across the BBB, and was defined as the BBB permeability index. In addition to the brain tissue, we also measured the enhancement kinetics of Gd-DTPA in the head muscle outside the brain for comparison and evaluation of the methodology.

Pearson correlation coefficients were calculated to determine if anatomical and vascular parameters varied as a function of age using SPSS for Windows and a significance level of 0.05.

RESULTS

Aged canines were impaired on a size-discrimination learning task but only a subset of old dogs performed poorly during object-approach learning and object-discrimination learning (14). Old dogs learned as well as younger dogs during reward approach learning, reversal learning and in the long-term retention test. The average test scores obtained from young (5 years and younger), middle aged (5–10 years) and old (10 years and older) dogs as a function of cognitive task are shown in Table 1.

Total cerebral volume, which included both cerebral brain tissue and CSF, was significantly correlated with the body weight of dogs ($r = 0.755$, $p < 0.0004$). To correct for this body size effect, measures of any single brain region were normalized to the total cerebral volume and expressed as a percent volume. The brains of old dogs exhibit pronounced ventricular enlargement and severe cortical atrophy, as shown in Fig. 1. These images were taken from slices through thalamus and hippocampus with the 3D SPGR pulse sequence. The brains of old dogs (9 and 15 years old) had large ventricles, deep gyri and widened sulci. The 6-year-old middle-aged dog had unusually large ventricles which were comparable to that of the 15-year-old dog, but no apparent cortical atrophy was observed. Figure 3 shows the correlation between the percent lateral ventricle volume (normalized to the total cerebral volume) and age, which was moderately dependent on age ($r = 0.484$, $p < 0.042$). However, the significance level was greatly improved after an outlier point obtained from the 6-year-old dog was removed ($r = 0.689$, $p < 0.002$). As shown in the figure, the age relationship is not linear because ventricle volume increases gradually until around the age of 10 years and subsequently shows a rapid increase. Correspondingly, cerebral brain-tissue volume decreased as a function of age ($r = -0.463$, $p < 0.071$). The cerebellum volume also decreased with age ($r = -0.467$, $p < 0.051$). The ranges of these volumetric measures and the statistical correlations with age are summarized in Table 2.

Vascular functional parameters were derived from a pharmacokinetic analysis of the enhancement kinetics. One 4-year-old dog, which displayed the fastest Gd-DTPA enhancement decay pattern, was chosen as the reference point against which all other dogs were compared for the vascular kinetics analysis. Figure 4 shows the enhancement kinetics measured from the brain tissue of the 4-year-old dog, a 9-year-old, and the 6-year-old outlier dog shown previously in Fig. 1. The respective vascular and interstitial

TABLE 1

COGNITIVE TEST SCORES[a] AS A FUNCTION OF AGE GROUP

Task	Young	Middle-Aged	Old
Reward Approach	8.3 (2.5)	8.25 (2.28)	11.37 (1.79)
Object Approach	1.0 (.25)	1.38 (.53)	3.0 (1.12)
Object Discrimination	12.2 (2.8)	8.75 (2.34)	9.87 (3.65)
Reversal Learning	40.4 (5.41)	32 (5.65)	30.1 (6.5)
Retention	13.0 (5.31)	11.0 (5.5)	7.25 (1.49)
Size Discrimination	9.0 (5.0)	18.46 (4.1)	29.0 (5.76)

[a] Mean (standard error of the mean).

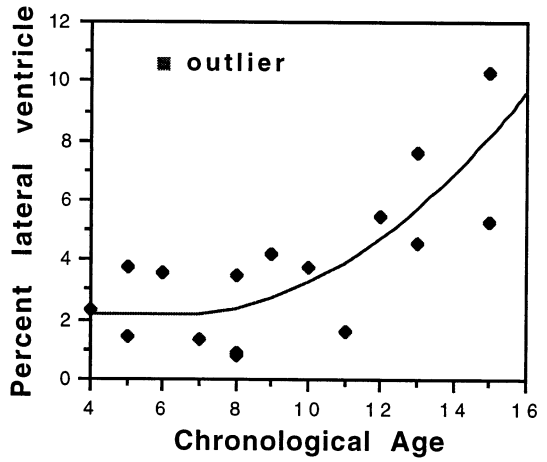

FIG. 3. The plot of percent lateral ventricle volume (normalized by the total cerebral volume) with age. The relationship with age was not linear, rather it was stable before age 10 and progressed very rapidly thereafter. A 6-year-old dog was obviously falling out of the age-dependence trend, and was marked as an outlier. Excluding the outlier, the age correlation was significant. The solid curve is for visual guidance.

kinetics, derived from pharmacokinetic analysis of the measured kinetics, are shown. Compared to the 4-year-old dog, the slower decay rate in the interstitial kinetics of the 9-year-old and 6-year-old dogs suggest that contrast agent is leaking through the BBB into the brain. In addition, whereas the vascular kinetics of these two dogs are comparable, the interstitial kinetics were greater in the 6-year-old than in the 9-year-old dog suggesting a greater breach in the BBB in the younger dog. The two vascular characteristic indices were measured for each individual dog, by defining the maximum enhancement in the vascular kinetics as the vascular volume index, and the ratio between the maximum enhancement in the interstitial kinetics to that in the vascular kinetics as the BBB permeability index. The age correlation of these two derived indices were studied. Neither the vascular volume ($r = 0.02$, $p =$ n.s.) nor the BBB permeability index ($r = 0.13$, $p =$ n.s.) were significantly correlated with age. However, after excluding the 6-year-old outlier, the BBB permeability showed improved correlation with age ($r = 0.35$, $p =$ n.s.). In contrast, the kinetics measured in the head muscle showed a clear age dependence ($r = 0.74$, $p < 0.001$). The age-dependence pattern was similar to that of the lateral ventricles shown in Fig. 1. The relationship was not a linear type; it was stable before age 10 then increased very rapidly.

The current sample of beagle dogs was included in a immunohistochemical study to determine the extent of β-amyloid pathology in different brain regions. The results of this study are reported elsewhere, but briefly, amyloid deposition typically does not occur before the age of 9 years (14,16). The exception to this was a 6-year-old dog showing diffuse senile plaques in the parietal and prefrontal cortices; this was the same dog that exhibited ventricular enlargement and BBB dysfunction described above. In addition, this dog obtained error scores in object discrimination (18 errors) and reversal learning (60 errors) that were outside the range of scores obtained by similarly aged dogs suggesting early cognitive dysfunction (15). Figure 5 shows that diffuse plaques were detected in the parietal lobe of this 6-year-old dog, which is comparable to the accumulation typically seen in an older dog. One possible mechanism underlying the BBB dysfunction in this dog is the accumulation of amyloid in the blood vessel walls.

TABLE 2

RANGES OF VOLUMETRIC MEASURES AND THE STATISTICAL CORRELATIONS WITH AGE

Region of Interest	Volume (cc)	% of Cerebral Volume	Age Correlation
Cerebral Region	57–79		
Cerebral Brain Tissue	47–69	80%–91%	$r = -0.463$ $p < 0.071$
Lateral Ventricles	0.5–5.5	1%–11%	$r = 0.689$ $p < 0.0002$[a]
Cerebellum	4.7–8.3	9%–12%	$r = -0.467$ $p < 0.051$

[a] Excluding the 6-year-old outlier.

DISCUSSION

MRI was used to study changes in anatomical and vascular characteristics of the canine brain as a function of age. The quality of the anatomical images acquired by the 3D SPGR pulse sequence allowed us to clearly differentiate CSF from gray and white matter (Fig. 2). In old dogs, we observed pronounced ventricular enlargement and severe cortical atrophy, which is similar to age changes seen in humans. The size of the lateral ventricles increased slowly until the age of 10 years and progressed very rapidly thereafter.

The kinetics of an MR contrast agent (Gd-DTPA) in the brain were measured using dynamic contrast-enhanced MRI to derive measures of cerebrovascular function. A pharmacokinetic analysis was performed to separate the vascular and interstitial kinetics to derive parameters representing vascular volume and BBB permeability. A segmentation algorithm was applied to differentiate CSF from the brain tissue (gray matter and white matter), utilizing their different signal intensities obtained from the anatomic images. The kinetics of contrast agent were measured from the brain tissue excluding CSF, thus any atrophic regions were excluded from the analysis. The procedure allowed us to derive vascular functions that were not biased by the degree of brain atrophy. This type of analysis would not be possible if two imaging modalities, e.g., using MRI to measure atrophy and using SPECT to measure perfusion, were involved. Therefore, although the vascular function parameters derived from MRI measurement do not carry absolute units, they still provide valuable information for spatially resolved comparisons in one subject or among different subjects. Harris et al. (13) has also demonstrated that the regional cerebral blood volume as measured by dynamic susceptibility contrast MRI (with a different contrast mechanism, T_2^* or ΔR_2^*) can differentiate the temporal-parietal deficit pattern in patients with AD compared to normal age-matched controls.

The vascular volume in the group of 18 dogs did not vary as a function of age and the BBB permeability index only showed a non-significant increase with age. These findings are not surprising, if we consider that in our definition of brain tissue, all associated atrophic regions were excluded. In humans, decreased cerebral blood flow (related to vascular volume) as a function of age is partly due to age associated cortical atrophy (11,25).

One interesting finding was that of a 6-year-old dog that had unusually large ventricles as well as BBB dysfunction. This particular dog also showed deposits of β-amyloid in the parietal cortex, which is unusual because amyloid deposition is not typically seen in beagle dogs under the age of 9 years (15,16). Although cortical atrophy was not apparent in this particular dog (Fig. 1D), with the serious problem of BBB damage we speculate that cortical atrophy may appear soon, and have some impact on cognitive function. The observation of a learning deficit in this dog

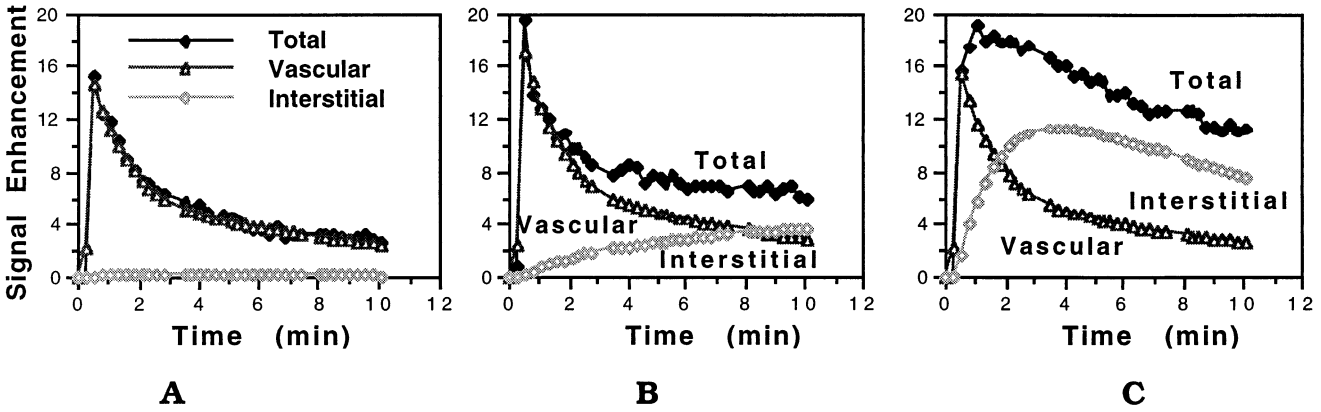

FIG. 4. The enhancement kinetics of Gd-DTPA measured in (*A*) a 4-year-old, (*B*) a 9-year-old, and (*C*) the 6-year-old outlier dog that had large ventricles. The kinetics in the 4-year-old displayed a fast decay pattern and it was assumed to be the standard against which other dogs were compared for the analysis of vascular kinetics. Based on data obtained from the standard dog, the kinetics measured in the 9-year-old and 6-year-old dogs were separated into vascular and interstitial kinetics. The vascular kinetics were comparable in these two dogs, but the interstitial kinetics in the 6-year-old was greater than in the 9-year-old. In fact, it was the highest among all dogs, suggesting a severe BBB-leakage problem.

relative to age-matched peers provides tentative support for this hypothesis (14).

The BBB may play an important role in brain aging and in age-related neurodegenerative disorders. In patients with AD, there is abundant evidence indicating morphological and biochemical abnormalities that implicate the break down of the BBB (1,2,3,17,18,21). These abnormalities include profound irregularities in the course of vessels and the vascular basement membrane, changes in specific proteins and receptors associated with the cerebral endothelium, degeneration of astrocytes, and increases in perivascular infiltrates. In the brain of the aged canine, Prior et al. present evidence of a complete loss of fluorescein diacetate (FDA) viability staining in some areas with vascular β-amyloid deposits, indicating the breakdown of vessel integrity (23). The MRI techniques demonstrated in the current study certainly open a door for a better understanding of the role of BBB in the aging process, and more specifically how it is related to the development of atrophy, neuropathology, and cognitive dysfunction. The dog also offers us unique insights into the relationships between in vivo measures of brain function, postmortem neuroanatomical measures and cognition because we can control and minimize the time interval between all these measures.

CONCLUSION

We demonstrate that anatomical and vascular characteristics of canine brain can be simultaneously studied within a single MRI session. As in humans, ventricular enlargement was the most pronounced feature in aged dogs. The relationship between ven-

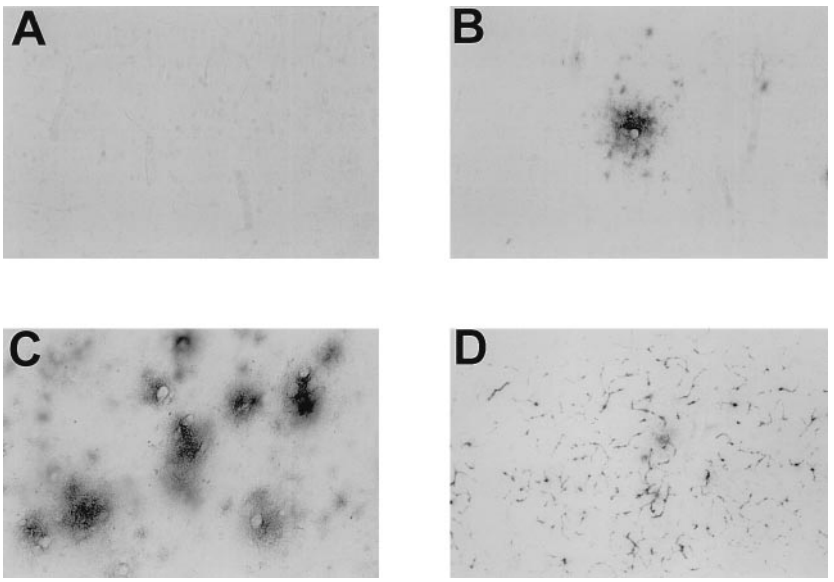

FIG. 5. β-amyloid immunoreactivity is typically absent as shown in one 6-year-old beagle dog (*A*) but another 6-year-old dog showing evidence of BBB dysfunction exhibited early onset pathology (*B*), which had not reached the levels of deposition seen in a 13-year-old dog in the same study (*C*). β-amyloid is also deposited in blood-vessel walls in the canine brain, which may be one mechanism leading to BBB dysfunction (*D*). Magnification: (*A–C*) 200×, (*D*) 40×.

tricle size and age was not linear, rather it was stable before age 10 and progressed very rapidly thereafter. The old dogs also exhibited deep gyri and widened sulci, indicating cortical atrophy. Vascular volume was not correlated with age however, BBB permeability measures showed a trend toward increasing permeability with age. MRI examination identified one middle-aged dog that showed early signs of aging, including enlarged ventricles and a severe BBB-leakage problem. Interestingly, this dog exhibited amyloid deposition at a much earlier age than that typically seen in beagle dogs. There was also an indication of early cognitive dysfunction on tests of learning and memory. These results suggest that dynamic contrast-enhanced MRI may provide useful information about the leakage status of BBB, that can aid in early diagnosis of pathological conditions. The canine model offers a unique opportunity to bridge the gap between noninvasive, in vivo measures of brain function and measures of postmortem neuropathology that will give us insight into differentiating normal from pathological aging.

ACKNOWLEDGEMENTS

This work was supported in part by National Institute on Aging Grant No. AG05142 and D/AG12694–02S1 and a fellowship to M.-Y. Su from University of California at Irvine-Markey Program in Human Neurobiology. The authors thank Dr. Mary Berry and Marjorie A. Billau for their assistance in the animal study, and Benito Montoya for his assistance in image acquisition.

REFERENCES

1. Blennow, K.; Wallin, A.; Fredman, P.; Karlsson, I.; Gottfries, C. G.; Svennerholm, L. Blood-brain barrier disturbance in patients with Alzheimer's disease is related to vascular factors. Acta Neurol. Scand. 81:323–326; 1990.
2. Buee, L.; Hof, P. R.; Bouras, C.; Delacourte, A.; Perl, D. P.; Morrison, J. H.; Fillit, H. M. Pathological alterations of the cerebral microvasculature in Alzheimer's disease and related dementing disorders. Acta Neuropathol. (Berl) 87:469–480; 1994.
3. Buee, L.; Hof, P. R.; Delacourte, A. Brain microvascular changes in Alzheimer's disease and other dementias. Ann. N.Y. Acad. Sci. 826:7–24; 1997.
4. Cummings, B. J.; Head, E.; Afagh, A. J.; Milgram, N. W.; Cotman, C. W. β-amyloid accumulation correlates with cognitive dysfunction in the aged canine. Neurobiol. Learn. Mem. 66:11–23; 1996.
5. Cummings, B. J.; Head, E.; Ruehl, W.; Milgram, N. W.; Cotman, C. W. The canine as an animal model of human aging and dementia. Neurobiol. Aging 17:259–268; 1996.
6. Cummings, B. J.; Su, J. H.; Cotman, C. W.; White, R.; Russell, M. J. β-amyloid accumulation in aged canine brain: A model of early plaque formation in Alzheimer's disease. Neurobiology 14:547–560; 1993.
7. Davis, P. C.; Mirra, S. S.; Alazraki, N. The brain in older persons with and without dementia: Findings on MR, PET, and SPECT images. Am. J. Roentgenol. 162:1267–1278; 1994.
8. Davis–Salinas, J.; Saporito–Irwin, S. M.; Cotman, C. W.; Van Nostrand, W. E. Amyloid β-protein induces its own production in cultured degenerating cerebrovascular smooth muscle cells. J. Neurochem. 65:931–934; 1995.
9. Frackowiak, J.; Mazur–Kolecka, B.; Wisniewski, H. M.; Potempska, A.; Carroll, R. T.; Emmerling, M. R.; Kim, K. S. Secretion and accumulation of Alzheimer's β-protein by cultured vascular smooth muscle cells from old and young dogs. Brain Res. 676:225–230; 1995.
10. Frackowiak, J.; Zoltowska, A.; Wisniewski, H. M. Non-fibrillar β-amyloid protein is associated with smooth muscle cells of vessel walls in Alzheimer disease. J. Neuropathol. Exp. Neurol. 53:637–645; 1994.
11. Garde, E.; Rostrup, E.; Larsson, H. B. W.; Paulson, O. B. Age-dependent cerebral circulation and brain volume measurements in healthy humans. Proceeding of the 5th ISMRM meeting. Vancouver, B.C. Canada; 1997:278.
12. Giacometti, A. R.; Davis, P. C.; Alazraki, N. P.; Malko, J. A. Anatomic and physiologic imaging of Alzheimer's disease. Clin. Geriatr. Med. 10:277–298; 1994.
13. Harris, G. J.; Lewis, R. F.; Satlin, A.; English, C. D.; Scott, T. M.; Yurgelun–Todd, D. A.; Renshaw, P. F. Dynamic susceptibility contrast MRI of regional cerebral blood volume in Alzheimer's disease. Am. J. Psychiatry 153:721–724; 1996.
14. Head, E.; Callahan, H.; Muggenburg, B. A.; Cotman, C. W.; Milgram, N. W. Visual-discrimination learning and β-amyloid accumulation in the dog. Neurobiol. Aging 19:415–425; 1998.
15. Head, E.; McCleary, R.; Lerner, K.; Muggenburg, B. A.; Milgram, N. M.; Cotman, C. W. Ruehl, W. W. A novel approach to determining the age of onset and rate of accumulation of amyloid protein in aging canine brain. W. W. ACVP/ASVCP Annual meeting in Albuquerque, NM; 1997.
16. Hou, Y.; White, R. G.; Bobik, M.; Marks, J. S.; Russell, M. J. Distribution of β-amyloid in the canine brain. NeuroReport 8:1009–1012; 1997.
17. Kalaria, R. N. The blood-brain barrier and cerebral microcirculation in Alzheimer disease. Cerebrovascular Brain Metabol. Rev. 4:226–260; 1992.
18. Kalaria, R. N.; Hedera, P. Differential degeneration of the cerebral microvasculature in Alzheimer's disease. Neuroreport 6:477–480; 1995.
19. Kawai, M.; Kalaria, R. N.; Cras, P.; Siedlak, S. L.; Velasco, M. E.; Shelton, E. R.; Chan, H. W.; Greenberg, B. D.; Perry, G. Degeneration of vascular muscle cells in cerebral amyloid angiopathy of Alzheimer disease. Brain Res. 623:142–146; 1993.
20. Kreiner, J. Reconstruction of neocortical lesions within the dog's brain: Instructions. Acta Biol. Exper. (Warsaw) 26:221–243; 1966.
21. Mecocci, P.; Parnetti, L.; Reboldi, G. P.; Santucci, C.; Gaiti, A.; Ferri, C.; Gernini, I.; Romagnoli, M.; Cadini, D.; Senin, U. Blood-brain-barrier in a geriatric population: Barrier function in degenerative and vascular dementias. Acta Neurol. Scand. 84:210–213; 1991.
22. Milgram, N. W.; Head, E.; Weiner, E.; Thomas, E. Cognitive functions and aging in the dog: Acquisition of nonspatial visual tasks. Behav. Neurosci. 108:67–68; 1994.
23. Prior, R.; D'Urso, D.; Frank, R.; Prikulis, I.; Pavlakovic, G. Loss of vessel wall viability in cerebral amyloid angiopathy. Neuroreport 7:562–564; 1996.
24. Su, M. Y.; Jao, J. C.; Nalcioglu, O. Measurement of vascular volume fraction and blood-tissue permeability constants with a pharmacokinetic model: Studies in rat muscle tumors with dynamic Gd-DTPA enhanced MRI. Magn. Reson. Med. 32:714–724; 1994.
25. Tanna, N. K.; Kohn, M. I.; Horwich, D. N.; Jolles, P. R.; Zimmerman, R. A.; Alves, W. M.; Alavi, A. Analysis of brain and cerebrospinal fluid volumes with MR imaging: impact on PET data correction for atrophy. Part II. Aging and Alzheimer dementia. Radiology 178:123–130; 1991.
26. Thomas, T.; Thomas, G.; McLendon, C.; Sutton, T.; Mullan, M. β-Amyloid-mediated vasoactivity and vascular endothelial damage. Nature 380:168–171; 1996.
27. Tofts, P. S. Modeling tracer kinetics in dynamic Gd-DTPA MR imaging. J. Magn. Reson. Imaging 7:91–101; 1997.
28. Wegiel, J.; Wisniewski, H. M.; Dziewiatkowski, J.; Tarnawski, M.; Nowakowski, J.; Dziewiatkowska, A.; Soltysiak, Z. The origin of amyloid in cerebral vessels of aged dogs. Brain Res. 705:225–234; 1995.
29. Wisniewski, H. M.; Frackowiak, J.; Mazur–Kolecka, B. In vitro production of β-amyloid in smooth muscle cells isolated from amyloid angiopathy-affected vessels. Neurosci. Lett. 183:120–123; 1995.